Joint Centre for Mesoscale Meteorology, Reading, UK

High-resolution analysis of frontal fracture

K. A. Browning
S. P. Ballard
C. S. A. Davitt

Internal Report No. 52

September 1995

Met Office Joint Centre for Mesoscale Meteorology Department of Meteorology
University of Reading PO Box 243 Reading RG6 6BB United Kingdom
Tel: +44 (0)118 931 8425 Fax: +44 (0)118 931 8791
www.metoffice.com

Designed and produced by the Met Office © Crown copyright 2001 01/0240 The Met Office logo is a registered trademark.

High-resolution analysis of frontal fracture

K.A. Browning*, S.P. Ballard and C.S.A. Davitt

Joint Centre for Mesoscale Meteorology

University of Reading, U.K.

[Submitted to Monthly Weather Review September 1995]

*Corresponding author address: K.A. Browning, Joint Centre for Mesoscale Meteorology, Harry Pitt Building, University of Reading, Whiteknights Road, PO Box 240, Reading RG6 6FN. (The Joint Centre for Mesoscale Meteorology is supported by the Meteorological Office and the Department of Meteorology, University of Reading).

ABSTRACT

A mesoscale array of dropwindsondes, released in a small rapidly-deepening frontal wave cyclone in the eastern North Atlantic during the FRONTS 92 experiment, has been assimilated into a 17km-grid mesoscale model nested within the Meteorological Office's operational Limited Area Model. The mesoscale model reproduced the evolving cloud pattern, with 'cloud head' and 'dry slot', seen in satellite imagery. It also revealed a well-defined evolution in the 3-dimensional thermodynamic structure associated with the process known as frontal fracture.

The frontal fracture was revealed most clearly in the pattern of wet-bulb potential temperature, θ_w, which was distorted by differential rotation, the rotation increasing with height. This led to backward-tilted θ_w-surfaces (and ana-cold frontal characteristics) in the cloud head to the north of the center of rotation, and to forward-tilted θ_w-surfaces (and kata-cold frontal characteristics) in the dry slot to the south of the center of rotation. The differential rotation was associated with a local maximum of potential vorticity aloft within a developing tropopause fold. The study does not address the issue of cause and effect.

1. Introduction

Shapiro and Keyser (1990) derived a frontal-cyclone life-cycle model (Fig 1) and they have used a 22.5km-resolution real-data simulation of a rapidly-deepening cyclone over the western North Atlantic to support it. They pointed out that, although the model differed from the classical Norwegian model (Bjerknes 1921, Bjerknes and Solberg 1922), it

resembled results from idealized numerical studies of amplifying baroclinic waves (eg Hoskins and West 1979, Keyser et al 1989, Schär 1989, Polavarapu and Peltier 1990). Their model contains four phases: (1) a broad baroclinic phase, (2) a frontal fracture phase, (3) a T-bone phase and (4) a warm-core seclusion phase. They showed that, 12 hours into the simulation, the previously continuous front fractured near the center of the deepening cyclone and the temperature gradients at the warm and cold fronts became sharp except in the immediate region of frontal fracture. As time progressed, the warm front developed backwards (in storm-relative coordinates) as a bent-back front, eventually encircling the cyclone center and perhaps secluding a pocket of warm air. Special observations obtained during project ERICA, for another rapidly developing cyclone, confirmed this sequence of events (Neiman and Shapiro 1993, Neiman et al 1993).

Meanwhile, awareness of rapidly deepening cyclones has also been growing in Europe, following the great October 1987 storm in SE England and northern France (Shutts 1990, Monk 1992). In many respects this storm was similar to the rapidly deepening cyclones off the eastern seaboard of the United States. Although in Europe storms of such severity are uncommon, a rather similar structure and evolution appears to apply to the frontal cyclones of moderate intensity that often affect NW Europe and the eastern North Atlantic (Bader et al 1995).

Browning and Roberts (1994) analysed a typical example of a small rapidly deepening frontal wave cyclone in NW Europe. They generated a model (Fig 2) that reconciles the frontal fracture model with the concepts of split fronts, conveyor belts, dry intrusion and cloud head. A key feature of this model is an intrusion of air from the upper troposphere

and lower stratosphere which is characterized by high potential vorticity (PV) and low wet-bulb potential temperature (θ_w). In the region of frontal fracture, this dry intrusion overruns a shallow moist zone (SMZ) of warm-conveyor-belt air as in the split-front model of Browning and Monk (1982). The dry intrusion, and its association with high PV, has been well known since the early studies of Reed (1955) and Danielsen (1964). Its association with rapidly deepening cyclones has been stressed by Uccellini (1990) and Young et al (1987).

An opportunity to deepen our understanding of the development of frontal wave cyclones in the eastern North Atlantic was provided in April 1992 by the FRONTS 92 experiment. During Intensive Observing Period (IOP) 3 of this experiment, the C130 Hercules aircraft of the UK Meteorological Research Flight (MRF) launched 58 dropwindsondes in a mesoscale array in the vicinity of a deepening cyclone center. The analysis of this dataset has proceeded in two ways: First, by the direct analysis of the observations, with the emphasis on the mesoscale sub-structure in the dry intrusion (Browning et al 1995). Second, as in the present paper, by the assimilation of the dropwindsonde profiles into a 17-km grid mesoscale model nested within the operational Meteorological Office Limited Area Model (LAM). Both analyses have highlighted the structure and evolution of the interface between the low-θ_w air of the dry intrusion and the moist high-θ_w airmass ahead of it.

The purpose of this paper is to use the mesoscale model results to describe and account for the evolution of the θ_w- interface just referred to, and the associated cloud features as seen by satellite. The emphasis is on the early stages of the rapid development of the cyclone , corresponding to Shapiro and Keysers' frontal fracture. Figure 3, showing

the model-derived field of dry-bulb potential temperature (θ) at 950mb, reveals the weak but characteristic signature of frontal fracture associated with the case to be presented below. However, as already mentioned, we shall be focusing on the θ_w-field (and relative humidity and cloud) for which the signature of frontal fracture shows up far more clearly. We shall demonstrate that the entire process leading to the overrunning dry intrusion and frontal fracture is related to the descent of an upper-level maximum of PV within a developing tropopause fold.

2. The model and data used in this study

a. Model description

This study uses versions of the UK Meteorological Office Unified Model (Cullen,1993). This hydrostatic, grid-point model using spherical polar coordinates can be run in global or limited-area configurations on a regular latitude-longitude grid at any desired horizontal or vertical resolution. Hybrid sigma/pressure co-ordinates are used in the vertical (Simmons and Burridge 1981). A conservative split-explicit integration scheme is used (Cullen and Davies 1991) and cloud water and ice are included as prognostic variables, making allowance for fractional cloud cover, after Smith (1990) (Smith 1994, Ballard and Hutchinson 1995). The co-ordinate pole can be rotated so that the equator runs through the area of interest, thus allowing more uniform resolution in limited-area configurations.

A full set of parameterizations is included in the model. The boundary-layer scheme is formulated in terms of conserved variables and so can represent both dry and cloudy boundary layers. It also includes a representation of non-local mixing (Smith 1994). Mixing coefficients are stability-dependent, using a moist Richardson number. Large-scale

precipitation is calculated in terms of the liquid water or ice content of the cloud and cooling of the atmosphere due to evaporation of precipitation is included (Smith 1990, Ballard and Hutchinson 1995, Gregory 1995). The annual cycle of radiation is imposed on the model which employs an interactive radiation scheme. The cloud optical properties depend on the predicted cloud water path and phase at both long-wave (Senior and Mitchell 1993) and short-wave (Slingo 1989). A mass-flux convection scheme with stability-dependent closure (Gregory and Rowntree 1990) is included which incorporates a representation of deep convective downdrafts (Gregory and Allen 1991). Surface hydrology and a soil-temperature model are also included (Dolman and Gregory 1992).

Although the above parameterizations were developed principally for climate simulations, which use coarse resolution eg 2.5° x 3.75° and 19 levels, the aim of the Unified Model project is to use the same model formulation in all configurations wherever possible. The same model is used for operational numerical weather prediction (NWP) at the UK Meteorological Office in global (0.8° x 1.25°, 19 levels), regional, known as LAM, (0.442° x 0.442°, 19 levels, 229x132 points, rotated pole at 30°N,160°E) and mesoscale (0.15° x 0.15°, 31 levels, 92x92, rotated pole at 37.5°N 177.5°E) configurations. The regional, high-resolution configurations are run operationally for a domain covering the North Atlantic and Europe in the case of the LAM , (see figure 4a), and an approximately 1500-km square domain centred on Britain and Ireland in the case of the mesoscale model. The ability of the model to produce satisfactory forecasts at mesoscale resolution was shown in Ballard et al (1993).

The Unified Model uses the analysis correction (AC) scheme (Lorenc et al 1991) for continuous assimilation of observations over a period at the start of the forecast by nudging the predicted values of wind, temperature and humidity towards the observed values.

b. Synoptic situation and available data

The cold-front wave that is the subject of this study was first identified on 25 April 1992, as a slow-moving feature about 1000km south-east of Newfoundland. The wave accelerated in an easterly direction with little or no development before deepening 12mb in 12 hours after 12UTC 27 April. The dropwindsondes, measuring wind, temperature and humidity (from about 500mb to the surface), were deployed from the MRF Hercules in the vicinity of the developing cyclone in the SW approaches to the UK between 12UTC and 21UTC 27 April, the period during which it underwent its most rapid development. The low tracked east-north-eastwards through the English Channel during the night of 27-28 April producing many hours of rain over southern England. Additional measurements were obtained from radiosondes launched from Larkhill between 13UTC 27 April and 13UTC 28 April and the large research radar at Chilbolton in southern England. These supplemented routine synoptic, satellite and radar data.

c. Experimental design

Operational forecasts of this event were available from the global and limited area (LAM) configurations of the Unified Model which at that time had 20 levels and used an early version of the model. However, the British Isles mesoscale configuration was not yet

operational and the location of the dropwindsondes was in any case outside its future operational area. In order to investigate the structure of the developing frontal wave observed during FRONTS 92 IOP3, data assimilation and forecast experiments were subsequently run at mesoscale resolution (0.15° x 0.15°, 32 levels) within an enlarged domain with shifted pole (140x140 points, rotated pole at 41.25°N 172.5°E), (see figure 4(a)). At 18UTC 27 April 1992 the entire frontal wave system and the dropwindsondes were within this mesoscale domain (figures (4b) and 4(c)).

In order to produce the best possible lateral boundary conditions for the mesoscale-resolution forecast, the operational observations were reassimilated into the global model in a continuous assimilation from 00UTC 26 April until 12UTC 28 April using a more recent, improved version of the Unified Model as described in section 2.1 (version 3.2 global, operational 11 January 1994). This assimilation sequence started from the 00UTC 26 April operational global analysis and the sea surface temperature from that time was used throughout. This global re-assimilation was used to provide boundary conditions for a continuous assimilation in the LAM configuration starting from the same global analysis. This again used a more recent version of the model (version 3.2 LAM, operational 7 December 1993). The operational data used in the global and LAM models consists of radiosonde temperature, wind and humidity, satellite temperature soundings (500km and LASS (Eyre and Jerrett 1982, Gadd 1994)), mean-sea-level pressure observations, surface winds from ships and buoys, satellite cloud-track winds, aircraft temperatures and winds, and 'bogus' data. The LAM continuous assimilation was also rerun to include the MRF Hercules dropwindsonde measurements of temperature, wind and humidity. This latter LAM

assimilation was then used to provide boundary and initial conditions for a mesoscale continuous assimilation from 00UTC 27 April to 12UTC 28 April.

The mesoscale assimilation used version 3.2 of the model, as operational on 7 December 1993, and the assimilation as implemented on 27 September 1994, but with some modifications to ensure a smoother analysis. The observations used in the mesoscale assimilation were basically the same as for the global and LAM configurations apart from the omission of 'bogus' data and high-resolution satellite sounding data (LASS), and the addition of wind, temperature and humidity data extracted from surface synop reports over land (Macpherson et al 1995). Unfortunately, it was not possible to adapt the detailed cloud analysis used operationally in the British Isles mesoscale model for this special-area research assimilation. The mesoscale continuous assimilation was however rerun to include the extra dropwindsonde data.

The impact of changes in the resolution of the Unified Model, and of the assimilation of additional dropwindsonde data, on the representation of the structure of this developing wave cyclone will be described elsewhere (Ballard et al 1995). For the purposes of this paper we shall limit ourselves to a mesoscale forecast run from initial data for 18UTC 27 April 1992 extracted from the mesoscale continuous assimilation including the dropwindsonde data. This forecast used boundary conditions from a LAM forecast run from initial data for the same time but extracted from the LAM continuous assimilation including the dropwindsonde data.

3. Validation of model performance

Before using the mesoscale model to provide a detailed diagnosis of the developing cyclone, it is necessary to show that it reproduces the main features realistically. Since we are concerned especially with the way in which the evolving thermodynamic structure leads to the development of features such as the cloud head, we shall begin by validating the model analysis and forecasts of the cloud-top temperature against the corresponding patterns inferred from Meteosat IR imagery. Later, in Sec 4(d), we shall also validate the model-derived precipitation against radar observations but this more subtle comparison is best left until after we have provided a full interpretation of the processes at work.

Fig 5 shows the cloud-top temperature derived from the mesoscale-model fields at 18UTC 27 April following an 18-hour period of data assimilation including the dropwindsonde data. This should be compared to the IR image in Fig 4(b). The model reproduces the main features of the observations, including the polar-front cloud-band with its rather sharp poleward-boundary and the cloud head south of Ireland, lowering toward the southwest. However, there is a tendency for it to overestimate the coldness of cloud tops, especially for the colder (higher) cloud where the difference is as great as 10-15°C. This is an effect that we have noticed on other occasions; we do not know whether it is due to the model overestimating the humidity at higher levels , the satellite underestimating the true coldness of the cloud tops because of the low emissivity of the cirrus cloud, or the simplified method of deriving cloud-top temperature from the model as the temperature at the highest level with 99% relative humidity with respect to ice. In any event, although we are concerned about this unresolved quantitative discrepancy, we are reassured by the models'

ability to reproduce the main pattern of the cloud, bearing in mind that only the sondes dropped between 12 and 18 UTC, and not the detailed imagery, were used as input to the model and that the sondes did not provide data at pressures lower than 500mb.

Further reassurance about the model's performance is provided by Fig 6 which compares the model's evolution with the observed evolution of the cloud head at 3-hourly intervals. The grey scales used in the imagery and model-derived fields have been tuned visually to highlight the significant features. With this adjustment, the two sequences appear rather similar. One feature that can just be discerned in both sequences is the tendency for the cloud head to propagate discontinuously, with a second cloud head (CH2) developing at the southwest end of the first cloud head (CH1), as shown schematically in the first column. In the model sequence, CH1 is the white area that travels from southwest Wales to the North Sea, whereas CH2 is related to the elongation of the light grey part of the overall cloud head which develops into a white area of cold cloud tops centred over Wales in the last frame of the sequence, at which time the imagery was showing white patches over SW England and north Wales associated with the same CH2, The double structure in the cloud head, although not immediately obvious in Fig 6, is clear when the data are viewed in higher resolution and false-colour. A reassuring feature of the model is how well it reproduces the evolution of the shallow southern end of CH2 in the last two time frames in Fig 6. This seemingly insignificant region of low cloud has been analysed in detail by Browning et al (1995) who show that it is dynamically a very interesting area where recently-descended dry-intrusion air was overrunning the surface cold fronts. We shall have more to say about this dry-intrusion air in the next section.

4. Evolution of the thermodynamic and dynamic fields responsible for the developing cloud head and dry slot

The developing cyclone was associated with a dry intrusion (dry slot) and cloud-head structure. We have shown that not only were these gross features reproduced by the model but that the mesoscale model was also able to discern the tendency for the cloud head to propagate discontinuously. Two cloud heads were identified, developing in succession. The purpose of the present section is to use the model to diagnose the associated evolution of the fields of wet-bulb potential temperature (θ_w), relative humidity and potential vorticity (PV), concentrating on just the second cloud head. Henceforth, when we refer to the cloud head, we shall be referring to CH2.

(a) *Evidence of differential rotation within the evolving θ_w-pattern*

An important structural change accompanying the development of the cyclone is revealed in the 9-hour time sequence of charts in Fig 7, which shows the evolution of the 9°C θ_w-surface at 950 and 700mb. Over the short period depicted in Fig 7, θ_w may be regarded as conserved and so, neglecting vertical advection, the change in shape of the θ_w-surface at one level relative to the other can be taken to be a measure of the differential advection between those levels. If one focuses on the region just south of the surface low-pressure centre L, a clear pattern of evolution emerges: the θ_w-isolines wind up cyclonically at both levels but the rate of rotation at 700mb significantly exceeds that at 950mb. Thus, in Fig 7, the most strongly backed portion of the solid line southwest of L, when averaged over 100km, rotates from a direction of 210-030° to 170-350° in 9 hours, whereas a

corresponding length of the dashed line rotates from 180-360° to 090-270° in the same period. In other words, the rate of rotation over 100km at 700mb (corresponding to a mean relative vorticity of $5x10^{-5}$ s^{-1}) was about twice as great at that level as it was at 900mb.

An important consequence of the differential rotation is that the slope of the θ_w-surface in Fig 7 changes sign in time and space. In the vicinity of the cyclone centre it starts off everywhere sloping upwards in the direction of the colder air: surfaces with lower θ_w are located below the 9°C θ_w-surface shown in Fig 7(a), with higher θ_w-surfaces above, and there is no potential instability. As time progresses, however, the differential rotation generates a region just on the southern side of the apparent center of rotation where the slope of the θ_w-surface reverses. In other words, it slopes upwards towards the warm air, and the low-θ_w air overruns a shallow zone of high-θ_w air, with resulting potential instability, in the stippled parts of Fig 7. Thus the front in this region resembles a kata-cold front, or split cold front, as described in the model of Browning and Monk (1982). The stippled region corresponds to what Browning and Monk defined as a shallow moist zone (SMZ). Elsewhere, notably to the north of the centre of rotation, the frontal structure resembles that of an ana-cold front. This distinction is highlighted in Fig 8, which shows that the overrunning air with low θ_w in the kata region is characteristically dry (the 'dry slot'), whilst the rearward-sloping ascent in the ana region to the north of it is responsible for the characteristic region of cloud and precipitation referred to as the cloud head.

(b) *The contrasting structure to the north and south of the apparent center of rotation*

The detailed 3-dimensional structure and evolution can be seen in the series of θ_w cross-sections in Fig 9. The top row shows sections orientated roughly north-south (NS) through the developing cloud head (the ana-cold frontal region) and the bottom row shows roughly west-east sections (WE) along the axis of the dry slot (the kata-cold frontal region).The locations are marked on Fig7. The stippled shading in the NS sections draws attention to the buckling of the 9°C θ_w-surface as a finger of moist, relatively high-θ_w, air ascends slantwise northwards within the cloud head. The WE sections depict a region of low-θ_w air at 700mb progressively overrunning higher-θ_w air; this same low-θ_w air begins to show up in the last two panels of the top row of NS sections near the position of the WE sections.

The corresponding evolution of the 3-dimensional humidity structure, is portrayed in Fig 10. The top row of NS sections depicts the tongue of moist air (stippled) forming the ascending part of the ana-cold frontal circulation that creates the cloud head. The bottom row of WE sections depict air in the dry intrusion overrunning the SMZ along the axis of the dry slot. (Successive pulses of drier air associated with the mesostructure of the cold front can be seen digging slightly into the SMZ. It is interesting that, even here, where the front is a kata-front characterised mainly by overrunning dry air, there is still a slight tendency for the formation of a shallow rearward-sloping circulation; however, this feature (which is analysed in detail in Browning 1995) was too shallow to generate significant precipitation.)

(c) *The generation of potential instability*

We have already drawn attention to the expanding region of potential instability corresponding to the SMZ in the stippled parts of Fig 7. The overrunning low-θ_w air in the dry intrusion that generated this potential instability was not only dry but also warm (Fig 11) because of its recent history of descent. This inhibited convection in the SMZ but, since this was itself a region of ascent, convection was able to break out at its leading edge. This is shown by the model-derived sequence of convective precipitation patterns in Fig 12(a-e). In the early stages of the developing cyclone, the model gave negligible convection, perhaps partly due to spin-up problems in the model. But after 28th/00UTC, a well-defined crescent-shaped area of convective precipitation formed at the leading edge of the SMZ. It is believed that this was associated with mid-level potential instability due to the buckling of the 9.5°C and 10°C θ_w-surfaces situated just ahead of the 9°C θ_w-surface, shown in Fig 9.

These processes are consistent with the set of images in Fig 13 in which the cross marks the location of the sounding in Fig 11. The dry intrusion shows up in the water vapour image (Fig 13(b)) as a dark zone which progressively lightens where the dry intrusion air ascends towards the east and north of X. The SMZ beneath the dry intrusion shows up bright in the visible image (Fig 13(c)) owing to extensive shallow cumulus convection in the boundary layer ahead of the surface cold front. The top of the SMZ was very low, as shown by the IR image (Fig 13(a)), and this is consistent with the absence of rain near X in the radar-network picture (Fig 13(d)).

(d) *Validation of the model-derived precipitation and convection within the cloud head*

Figure 12(e) extends the model sequence to 28th/06UTC, beyond the period described in earlier figures, and when the cloud-head precipitation was over southern England. This enables a comparison to be made with detailed 3-dimensional precipitation measurements obtained with the Chilbolton radar as well as the UK radar network and surface synoptic observations, all shown in Fig 12(f). The Chilbolton radar was performing range-height scans at a series of azimuths and, because of its narrow (¼ deg) beamwidth, it was able to identify clearly not only the overall area of precipitation but also the lateral extent of the region of convective cells. The overall agreement with the model is good but there are interesting differences in detail. Both model and observations show areas of convective precipitation associated with the cloud head, particularly in its southern part. However, despite excellent agreement between the model and radar network on the northward extent of the overall surface precipitation at that time, the model's convective precipitation is predicted to be further south and east than the region of convective activity derived from the vertically scanning radar at Chilbolton. This may be related to a slight eastward displacement of the forecast low center relative to the analysed position which is also reflected in the eastward displacement of the convective precipitation over France. However, it could also be that the model is underestimating the amount of cyclonic rotation, or that the model's ascent is triggering the convection prematurely, ie too far south. In fact the observed region of convective activity shows much better agreement with the model's predicted area of maximum resolved (stratiform or dynamic) rainfall (not depicted in figure 12). It is possible that, at the model resolution used in this study, some of the convective processes are being expressed explicitly in terms of gridscale ascent rather than being parameterized.

(e) *The upper-level potential vorticity anomaly associated with the developing cloud head and dry slot*

We have described above the structural changes accompanying a process of differential rotation, especially in regard to its effect on the distribution and type of cloud and precipitation. Although we have concentrated on the behaviour of the lower troposphere, and in particular have focused on the differential rotation between the 950 and 700mb levels, it is significant that this was closely associated with the downward penetration of an upper-level maximum in potential vorticity (PV). Fig 14, showing a perspective view looking from north to south, depicts the PV=1.5 surface (conventional PV units). A PV value of 2 corresponds to the dynamical tropopause and this 1.5 PVU-surface originates very close to it. The 3-dimensional portrayal gives a strong impression of a surface undergoing cyclonic rotation as it extends downwards towards the jungle of minor PV maxima which are likely to have been generated diabatically in the moist low-level flow ahead of the system (to the left of this diagram). A roughly north-south section through the major upper-level PV anomaly (Fig 15(a)) shows the 1.5 PVU-surface protruding down towards one of the diabatically generated maxima at low levels.

We have little doubt that the developing differential rotation below 700mb referred to earlier was associated with the downward penetration of this upper-level PV maximum. However, a determination of the precise effect of the upper-level PV anomaly on the pattern of rotation and vertical velocity in the lower troposphere, and the reverse effect of the low-level PV anomaly on the higher levels, requires a detailed attribution study which is beyond the scope of the present paper.

5. Conclusions

This study of a small rapidly-deepening cyclone in the eastern North Atlantic has shown that the early phase of frontal fracture as described by Shapiro and Keyser (1990) has a clear signature in the 3-dimensional field of wet-bulb potential temperature, θ_w. Essentially the evolution of the θ_w-pattern can be accounted for in terms of the distortion due to differential rotation. This was associated with the downward penetration of a local maximum of potential vorticity within a developing tropopause fold. The present study has not dealt explicitly with the dynamics of the interaction of the upper-level potential vorticity with the low-level baroclinicity. Thus we are not able to attribute cause and effect. All we can say at this stage is that there is a clear association of the upper-level PV anomaly with the differential rotation: parts of the θ_w-field closer to the upper-level PV anomaly rotate faster than the θ_w-field lower down.

The differential rotation leads to backward-tilted θ_w-surfaces (and hence ana-cold frontal characteristics) to the north of the center of rotation, and to forward-tilted θ_w-surfaces (and kata-cold frontal characteristics) just to the south of the center. Rearward-sloping ascent in the northern part leads to the generation of the 'cloud head'. In the southern part, dry intrusion air with low θ_w overrides a shallow moist zone (SMZ) of high-θ_w air, as in the split-cold-front model of Browning and Monk (1982), and this leads to the generation of a characteristic dry slot as seen in the satellite imagery.

The overrunning of the dry intrusion above the SMZ generates potential instability. Above much of the SMZ the low-θ_w air is characterised by a relatively high dry bulb

potential temperature owing to its earlier descent and so convection is confined to shallow cumulus. This is, however, a region of broad-scale ascent ahead of the upper-level vortex and, at the northern and eastern edges of the SMZ, convection breaks through into the middle troposphere. In the present case this is most pronounced along the southern edge of the cloud head. Validation against satellite and radar data shows that, after allowing for positional errors in the model forecasts, the processes leading to convection were well represented by the mesoscale model used in this study. The dependence of the predictions on model resolution and other factors will be evaluated in a separate paper (Ballard et al 1995).

Acknowledgements Many people were involved in the FRONTS 92 experiment and we are grateful to all who contributed to its success. In particular, we thank the dropwindsonde team of Andy Macallan and Vic Lissaman, the scientific staff led by Sid Clough and the aircrew of the Meteorological Research Flight for their role in developing the observing systems and making the observations and John Bray for processing the dropwindsondes for inclusion in the Unified Model data assimilation scheme. We are also grateful to Anthony Illingworth for providing data from the Chilbolton radar, Nigel Roberts for analysing the radar data , Bruce Macpherson, Bruce Little, Greg Bason and Adam Maycock for providing guidance on setting up the data assimilation and Gerard Hutchinson for setting up the initial Global and LAM re-assimilation, carrying out initial forecast runs and investigations and providing diagnostic facilities. Further information and documentation on the Unified Model can be obtained from the authors or NWP Division, Meteorological Office, London Road, Bracknell, UK.

References

Bader, M.J., G.S. Forbes, J.R. Grant, R.B.E. Lilley and A.J. Waters, 1995: *Images in weather forecasting*. Cambridge University Press. In press.

Ballard, S.P., R. Robinson, R.T.H. Barnes, S. Jackson and S. Woltering, 1993 Development and performance of the new mesoscale model, *Forecasting Research Technical Report* No 40, available from National Meteorological Office Library, London Road, Bracknell, Berkshire RG12 2SZ.

Ballard, S.P., and M.G. Hutchinson, 1995 : Parametrization of mixed-phase cloud and precipitation. proceedings of ECMWF workshop on 'Modelling, validation and assimilation of clouds', held 31 October to 4 November 1994 at Shinfield Park, Reading

Ballard, S.P., C.S.A. Davitt, J. Bray, M.G. Hutchinson, K.A. Browning, and N.M. Roberts, 1995: Representation of the structure of a developing frontal wave in an NWP model. In preparation

Bjerknes, J., and H. Solberg 1922: Life cycle of cyclones and the polar front theory of atmospheric circulation. *Geofys. Publ.*, **3**, 1-18

Bjerknes, V., 1921: On the dynamics of the circular vortex with applications to the atmosphere and atmospheric vortex and wave motions. *Geofys. Publ.*, **2**, 1-88

Browning, K.A., 1995: On the nature of the mesoscale circulations at a kata-cold front, *Tellus A*, In press

Browning, K.A., and G.A. Monk, 1982: A simple model for the synoptic analysis of cold fronts, *Quart.J.Roy.Meteor.Soc.*, **108**, 435-452.

Browning, K.A., and N.M. Roberts, 1994: Structure of a frontal cyclone, *Quart.J.Roy.Meteor.Soc.*, **120**, 1535-1557.

Browning, K.A., S.A. Clough, C.S.A. Davitt, N.M. Roberts, T.D. Hewson and P.G.W. Healey, 1995: Observations of the mesoscale sub-structure in the cold air of a developing frontal cyclone, *Quart.J.Roy.Meteor.Soc.*, **121**, 1229-1254.

Cullen, M.J.P., 1993: The Unified Forecast/Climate Model. *Meteorol. Mag.*, **122**, 81-94.

Cullen, M.J.P. and T. Davies,1991: A conservative split-explicit integration scheme with fourth order horizontal advection. *Quart.J.Roy.Meteor.Soc.*, **117**, 993-1002.

Danielsen, E.F., 1994: Project Springfield Report, Defense Atomic Support Agency. Washington D.C. 20301, DASA 1517 (NTIS # AD-607980), 97 pp

Dolman, A.J. and D. Gregory, 1992: The parametrization of rainfall interception in GCMs., *Quart.J.Roy.Meteor.Soc.*, **118**, 455-467.

Eyre, J.R. and D.Jerrett, 1982: Local area atmospheric sounding for satellites. *Weather,* **37**, 314-322.

Gadd,A.J. 1994: Assimilation of TOVS data at the UK Met Office. Proceedings of ECMWF/EUMETSAT workshop on Developments in the use of satellite data in numerical weather prediction, held 6-10 September 1993 at Shinfield Park, Reading, UK.

Gregory,D. and S. Allen, 1991: The effect of convective scale downdraughts upon NWP and climate simulations., Preprints of the 9th Conf. on Numerical Weather prediction, Oct 14-18, 1991, Denver, Co., USA.

Gregory, D. and P.R. Rowntree, 1990: A mass flux convection scheme with representation of cloud ensemble characteristics and stability dependent closure., *Mon. Wea. Rev.*, **118**, 1483-1506.

Gregory, D. 1995: A consistent treatment of the evaporation of rain and snow for use in large-scale models. To appear in *Mon. Wea. Rev.*

Hoskins, B.J., and N.V. West, 1979: Baroclinic waves and frontogenesis. Part II: Uniform potential vorticity jet flows - cold and warm fronts. *J.Atmos.Sci.*, **36**, 1663-1680

Keyser, D., B.D. Schmidt, and D.G. Duffy, 1989: A technique for representing three-dimensional vertical circulations in baroclinic disturbances. *Mon.Wea.Rev.*, **117**, 2463-2494

Lorenc,A.C., R.S. Bell and B. Macpherson, 1991: The Meteorological Office analysis correction data assimilation scheme. *Quart.J.Roy.Meteor.Soc.*, **177**,59-89.

Macpherson, B., B.J. Wright, W.H. Hand and A.J. Maycock, 1995 'The Meteorological Office mesoscale data assimilation scheme', Forecasting Research Division Scientific Paper No 33, available from National Meteorological Office Library, London Road, Bracknell, Berkshire RG12 2SZ and submitted to *Quart.J.Roy.Meteor.Soc.*

Monk, G.A., 1992: Synoptic and mesoscale analysis of intense mid-latitude cyclones, *Meteor.Mag.*, **121**, 269-283

Neiman, P.J., and M.A. Shapiro, 1993: The life cycle of an extratropical marine cyclone. Part I: Frontal-cyclone evolution and thermodynamic air-sea interaction. *Mon.Wea.Rev.*, **121**, 2153-2176

Neiman, P.J., M.A. Shapiro and L.S.Fedor, 1993: The life cycle of an extratropical marine cyclone. Part II: Mesoscale structure and diagnostics. *Mon.Wea.Rev.*, **121**, 2177-2199

Polavarapu, S.M., and W.R. Peltier, 1990: The structure and non-linear evolution of synoptic scale cyclones: Life cycle simulations with a cloud-scale model. *J.Atmos.Sci.*, **47**, 2645-2672

Reed, R.J., 1955: A study of a characteristic type of upper level frontogenesis. *J.Meteor.*, **12**, 226-237

Schär, C.J., 1989: Dynamische Aspekte der aussertropischen Zyklogenese, Theorie und numerische Simulation in Limit der balancierten Stromungssysteme. Dissertation Nr. 8845 der Eidgenossischen Technischen Hochschule, Zurich, 241 pp

Shapiro, M.A., and D. Keyser, 1990: Fronts, jet streams, and the tropopause. *Extratropical Cyclones, The Erik Palmén Memorial Volume*, C.W. Newton and E. Holopainen, Eds., Amer.Meteor.Soc., 167-191

Shutts, G.J., 1990: Dynamical aspects of the October storm, 1987: A study of a successful fine-mesh simulation, *Quart.J.Roy.Meteor.Soc.*, **116**, 1315-1347

Senior, C.A. and J.F.B. Mitchell, 1993: Carbon dioxide and climate: the impact of cloud parametrization. *J.Climate*, **6**, 393-418.

Simmons,A.J. and D.M. Burridge, 1981: An energy and angular momentum conserving finite difference scheme and hybrid coordinates. *Mon. Wea. Rev.*, **109**, 758-766.

Slingo, A., 1989: A GCM parametrization for the shortwave radiative properties of clouds. *J. Atmos. Sci.*, **46**, 1419-1427

Smith, R.N.B., 1990 : A scheme for predicting layer clouds and their water content in a general circulation model. *Quart. J. Roy. Meteor. Soc.*, **116** , 435-460.

Smith, R.N.B., 1994 : Experience and developments with the layer cloud and boundary layer mixing schemes in the UK Meteorological Office Unified Model. proceedings of ECMWF workshop on 'Parametrization of the cloud topped boundary layer', held 8-11 June 1993 at Shinfield Park, Reading

Uccellini, L.W., 1990: Processes contributing to the rapid development of extratropical cyclones. *Extratropical Cyclones, The Erik Palmén Memorial Volume*, C.W. Newton and E. Holopainen, Eds., Amer.Meteor.Soc., 81-105

Young, M.V., G.A. Monk and K.A. Browning, 1987: Interpretation of Satellite Imagery of a rapidly deepening cyclone. *Quart.J.Roy.Meteor.Soc.*, **113**, 1089-1115

Figure Legends

Fig 1 Model of frontal-cyclone evolution (Shapiro and Keyser 1990). Phase I: incipient broad-scale baroclinic zone. Phase II: frontal fracture. Phase III: bent-back front and frontal T-bone. Phase IV: warm-core frontal seclusion. Upper sequence: sea-level pressure (solid), fronts (bold) and cloud signature (shaded). Lower sequence: temperature (solid), and cold and warm air currents (solid and dashed arrows, respectively).

Fig 2 Structure of rapidly-deepening frontal cyclone in NW Europe at stage of frontal fracture (Browning and Roberts 1994). See key for details.

Key to Fig 2: Explanation of the analysis scheme in Fig 2

sea level isobars

edge of major cloud features

(cloud head, thinly stippled; polar front cloud, thickly stippled: rain, large dots)

boundary of dry intrusion

(the dry intrusion is seen as a dry slot in the satellite imagery; it overruns a shallow moist zone of higher θ_w and undercuts rear edge of polar front cloud)

surface warm front (cold-conveyor-belt air ahead of the warm front has a system-relative motion towards the west and contributes to most of the precipitation-producing ascent within the cloud head).

sharp surface cold front (SCF), associated with a sharp wind veer, an abrupt drop in θ_w and narrow line convection. (The sharp SCF is in two parts, the northern part being a bent-back extension of the warm front).

diffuse surface cold front
(no abrupt changes, no precip., no cloud signature) (the surface cold front in this location may sharpen during subsequent deepening of the cyclone as air from the cold conveyor belt sweeps around the southern flank of the cyclone center).

upper cold θ_w-front (UCF), marking leading edge of dry intrusion. (The UCF is always detectable as a θ_w-front but there may not be a significant θ-gradient.)

300 mb jet axis in the vicinity of its core.

jet core, (in the region of deceleration ahead of J there is an indirect ageostrophic circulation, in which boundary-layer air

from the warm conveyor belt flows towards the cyclone center, ascends at the line convection and then forms the top of the eastern part of the cloud head).

shallow moist zone (SMZ)

SMZ

(region between the UCF and SCF where moist high-θ_w air in the boundary layer, originating in the warm conveyor belt, is overrun by the lower-θ_w dry intrusion).

Fig 3 Dry-bulb potential temperature derived from mesoscale model at 950 mb at 00 UTC 28 April (T + 6 forecast). X marks location of forecast low centre.

Fig 4 (a) Domain of the Meteorological Office Limited Area Model, with mesoscale model domain used for this study overlain. (b) Meteosat infra-red image for 18 UTC 27 April covering the mesoscale model domain. The overlay shows the area containing the dropwindsondes, with a msl pressure analysis derived from ship observations. (c) Zoomed Meteosat infra-red image for 18 UTC 27 April covering the dropwindsonde area. Black dots show the position of individual sondes.

Fig 5 Cloud-top temperature derived from the mesoscale model at 18 UTC 27 April (T+0 analysis).

Fig 6 Time sequence of cloud-top temperature as observed and as derived from the mesoscale model

Rows (a) 18 UTC 27 April (T+0), (b) 21 UTC 27 April (T+3)

(c) 00 UTC 28 April (T+6), (d) 03 UTC 28 April (T+9)

Columns (i) Schematic diagrams showing two cloud heads derived from the mesoscale model

(ii) Cloud-top temperatures derived from mesoscale model

(iii) Meteosat infra-red image

Note that there are (intentionally) different grey scales in (ii) and (iii): in the former, white represents temperatures below -40°C whilst in the latter it represents temperatures below -30°C.

Fig 7 Three-hourly sequence of the 9°C wet-bulb potential temperature at 950 mb (solid contours) and 700 mb (dashed contours), as derived from the mesoscale model. (a) 18 UTC 27 April (T+0), (b) 21 UTC 27 April (T+3)

(c) 00 UTC 28 April (T+6), (d) 03 UTC 28 April (T+9)

Stippled shading draws attention to a region of potential instability where the dashed contour runs ahead of the solid contour. L is the position of the surface low. V marks the position of the potential vorticity maximum at 600 mb. NS and WE show the locations of cross-sections in Figs 9 and 10.

Fig 8 Schematic diagram for 00 UTC 28 April, based on the mesoscale model forecast T+6, showing cloud head 2 (dotted shading), dry air (RH < 30%) at

700 mb (dashed shading), fronts, and 9°C wet-bulb potential temperature contours at 950 mb (solid) and 700 mb (dashed).

Fig 9 Three-hourly sequence of cross-sections of wet-bulb potential temperature derived from the mesoscale model forecast, with $\theta_w > 9°C$ shaded.

Columns (a) 18 UTC 27 April (T+0), (b) 21 UTC 27 April (T+3)
(c) 00 UTC 28 April (T+6)

Rows Top: Approximately north-south sections, NS
Bottom: Approximately west-east sections, WE

Each section is 650 km long. Vertical lines in the cross sections show where the two sections cross. The locations of the cross-sections are plotted in Fig 7.

Fig 10 As for Figure 9 except for relative humidity. Contours for RH = 30, 60 and 90%, stippled above 90%.

Fig 11 Model-generated tephigram in the Shallow Moist Zone, at the location shown in Fig 13.

Fig 12 (a-e) Three-hourly sequence from 18 UTC 27 April (T+0) to 06 UTC 28 April (T+12) of the convective precipitation diagnosed from the mesoscale model forecast, superimposed on the model-derived 9.5°C wet-bulb potential temperature contours at 950mb (dashed contour) and 700mb (dotted contour). Precipitation intensities greater than 0.1 and 0.4 mm h^{-1} are shown grey and

black respectively. In (e) the area with total forecast precipitation rate greater than 0.1mm h^{-1} is also shown as the lightly shaded region.

(f) Area of convection at 06 UTC 28 April, deduced from the elevation-scanning radar at Chilbolton is shown as the dark shaded region. The dashed line marks the outer range of the radar. The area with surface precipitation rate greater than about 0.1mm h^{-1} ,as derived from the UK FRONTIERS radar network, is shown as the lightly shaded region. The edge of the UK radar network is shown as a solid line. Symbols representing surface significant weather reports are shown over continental Europe where x means no precipitation reported, v rain shower, · ·· : ∴ slight to moderate intermittent and continous precipitation and ,, drizzle.

Fig 13 Meteosat imagery for 06 UTC 28 April: (a) infra-red, (b) water vapour, and (c) visible channel. Panel (d) shows European radar network data obtained through COST (Cooperation in Science and Technology) at 07 UTC 28 April.

Fig 14 Three-dimensional view of the potential vorticity = 1.5 PVU isosurface from the mesoscale model forecast, looking from the north.

(a) 21 UTC 27 April (T+3), (b) 00 UTC 28 April (T+6)

(c) 03 UTC 28 April (T+9), (d) 06 UTC 28 April (T+12)

Fig 15 Pattern of potential vorticity at 00 UTC 28 April derived from the mesoscale model:

(a) cross-section along N′S′ marked in (b), with PV values greater than 1.5 PVU shown shaded,

(b) plan view of PV showing areas of high level origin greater than 1.5 PVU at 400, 500, 600 and 700 mb (stippled) and diabatically-generated areas of low level origin greater than 1.0 PVU at 900 mb (hatched).

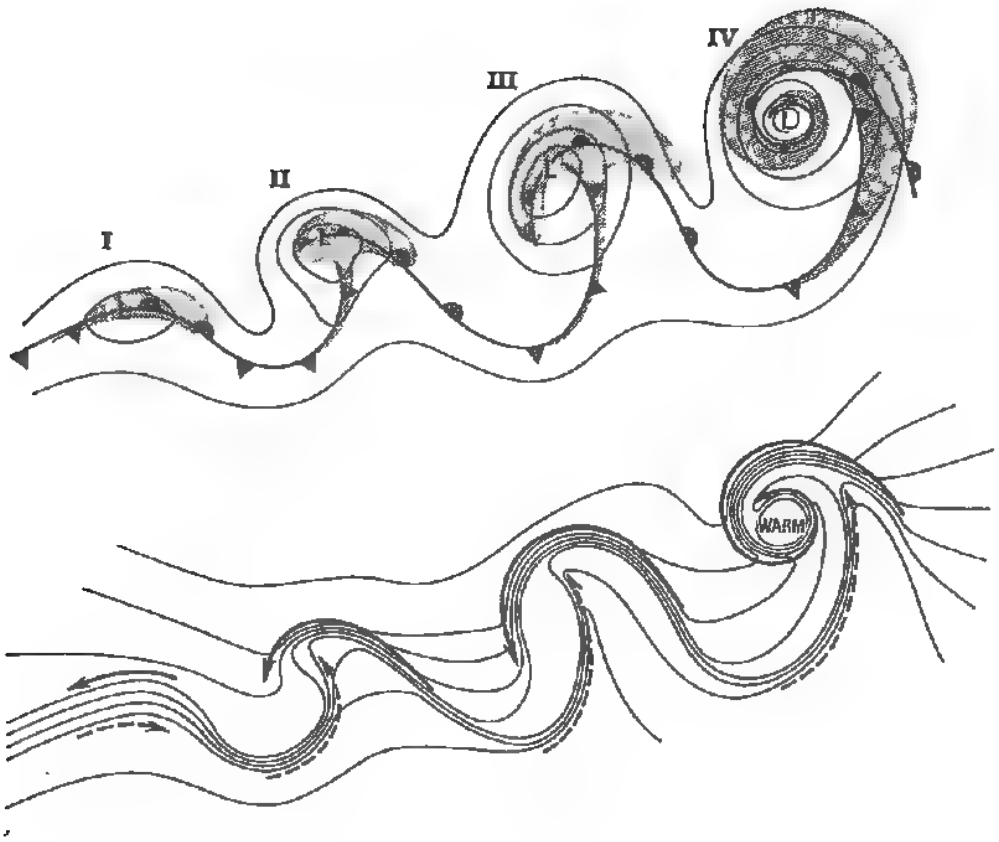

Figure 1

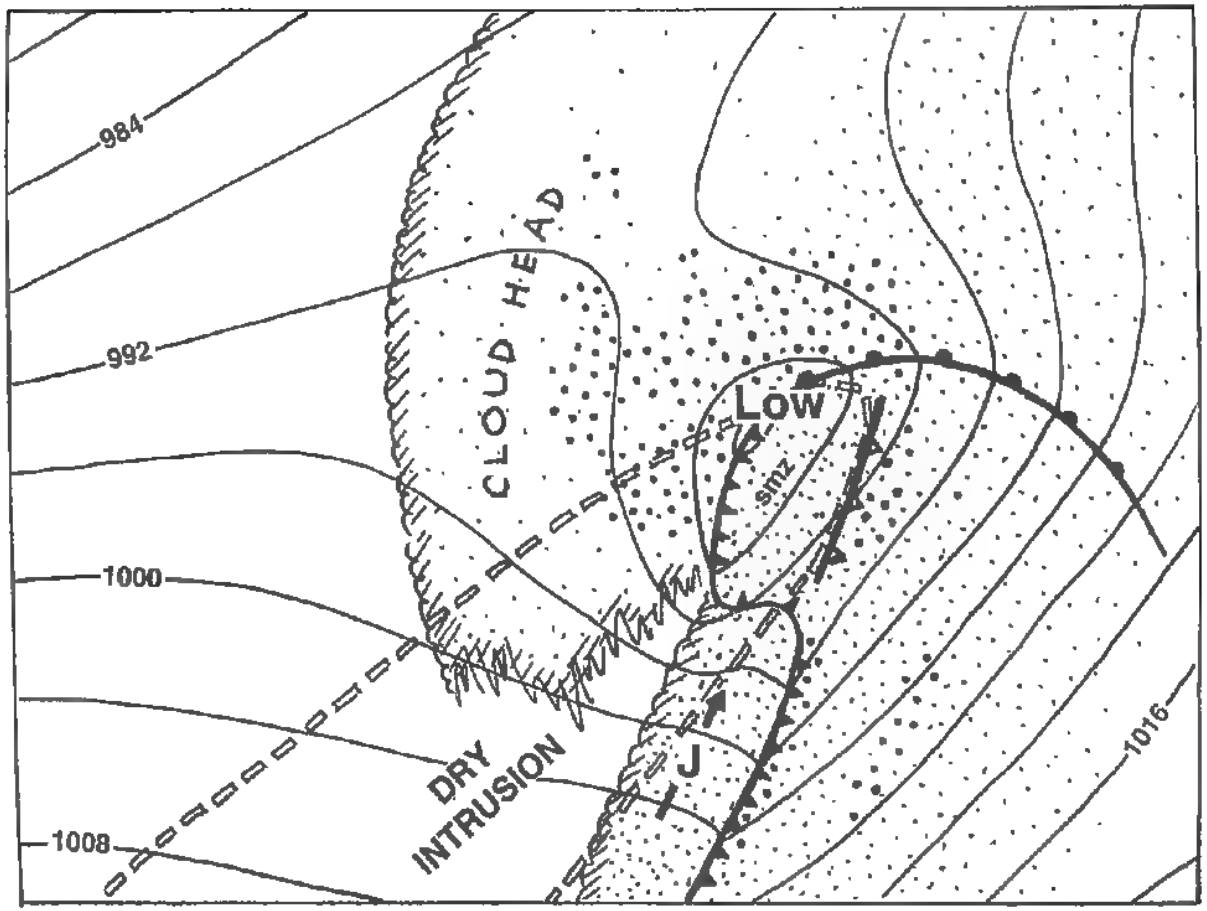

Figure 2

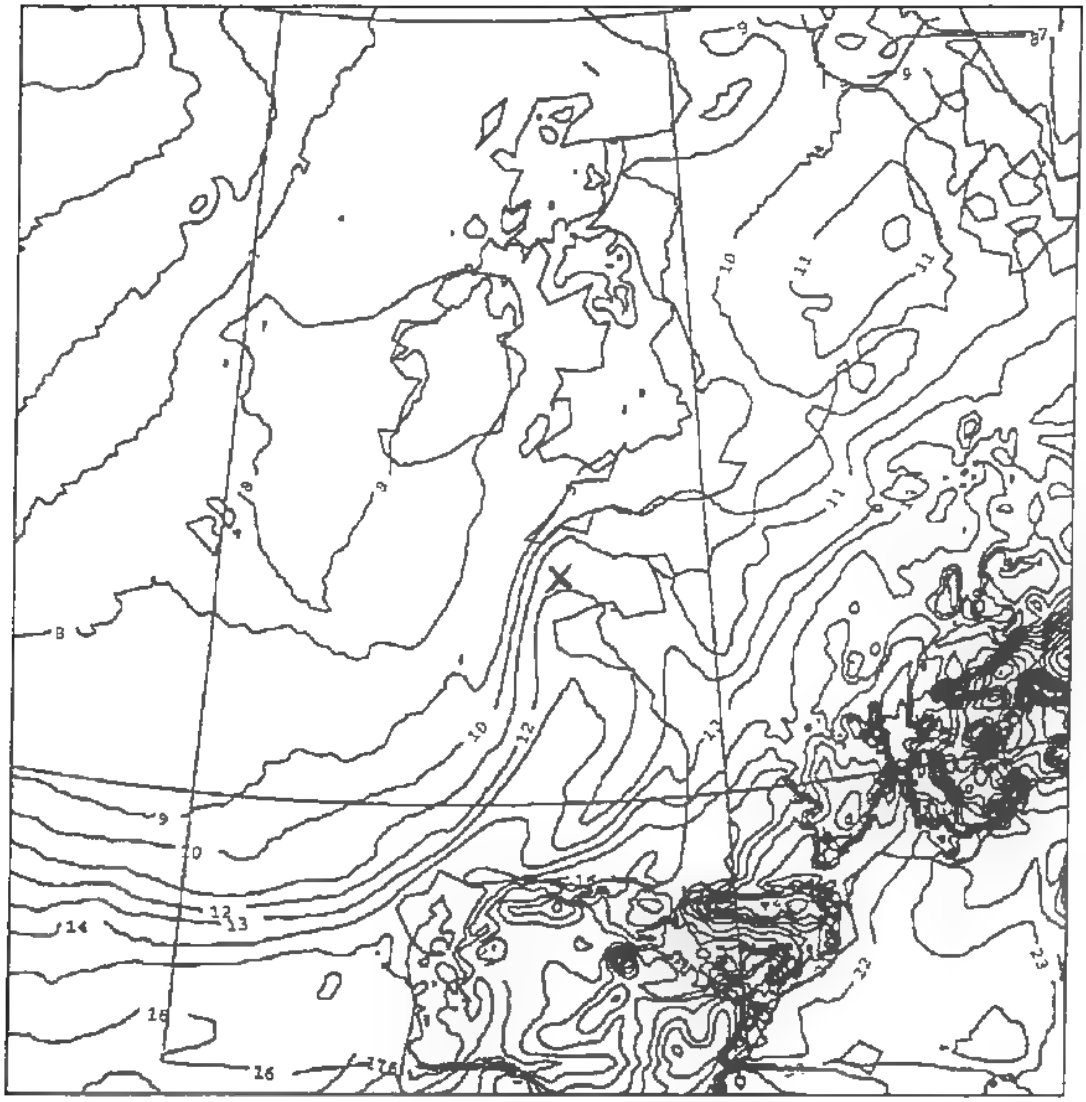

Figure 3

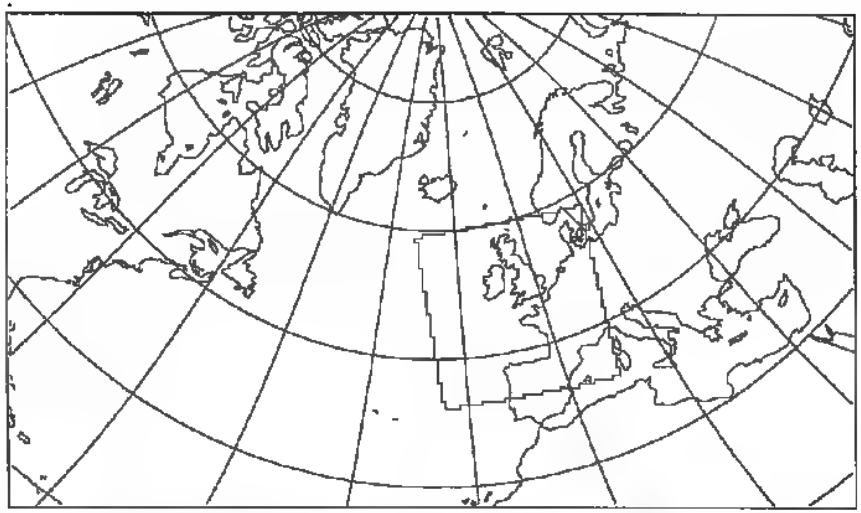

(a)

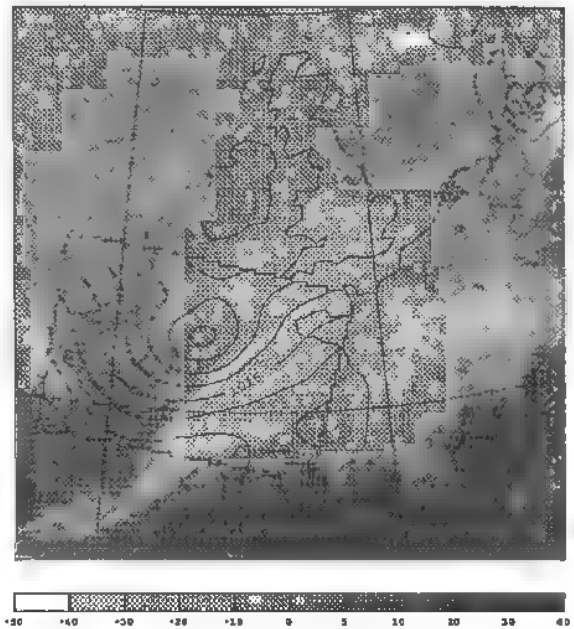

(b)

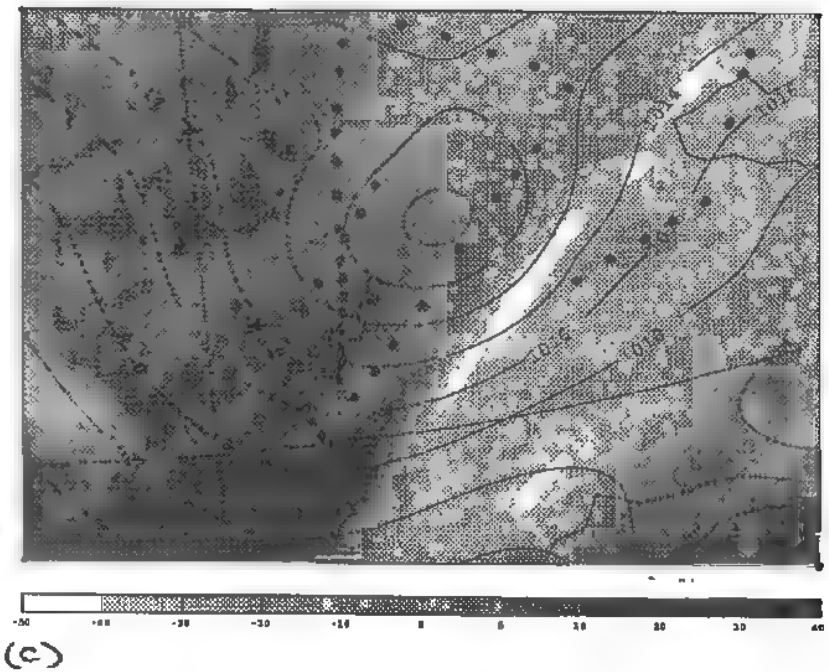

(c)

Figure 4

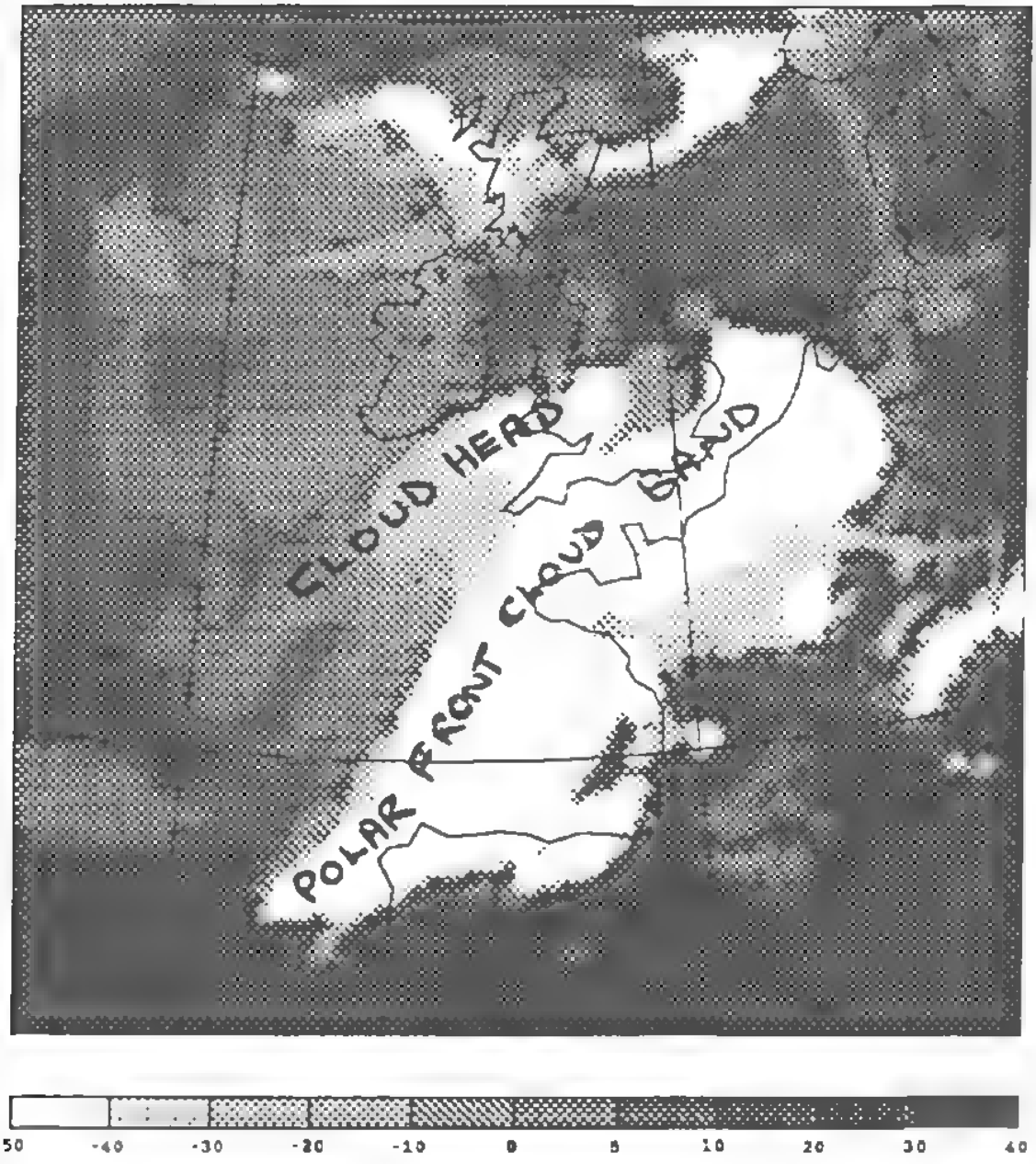
CLOUD HERD
CLOUD BAND
POLAR FRONT CLOUD
50
-40
-30
-20
-10
0
5
10
20
30
40

Figure 5

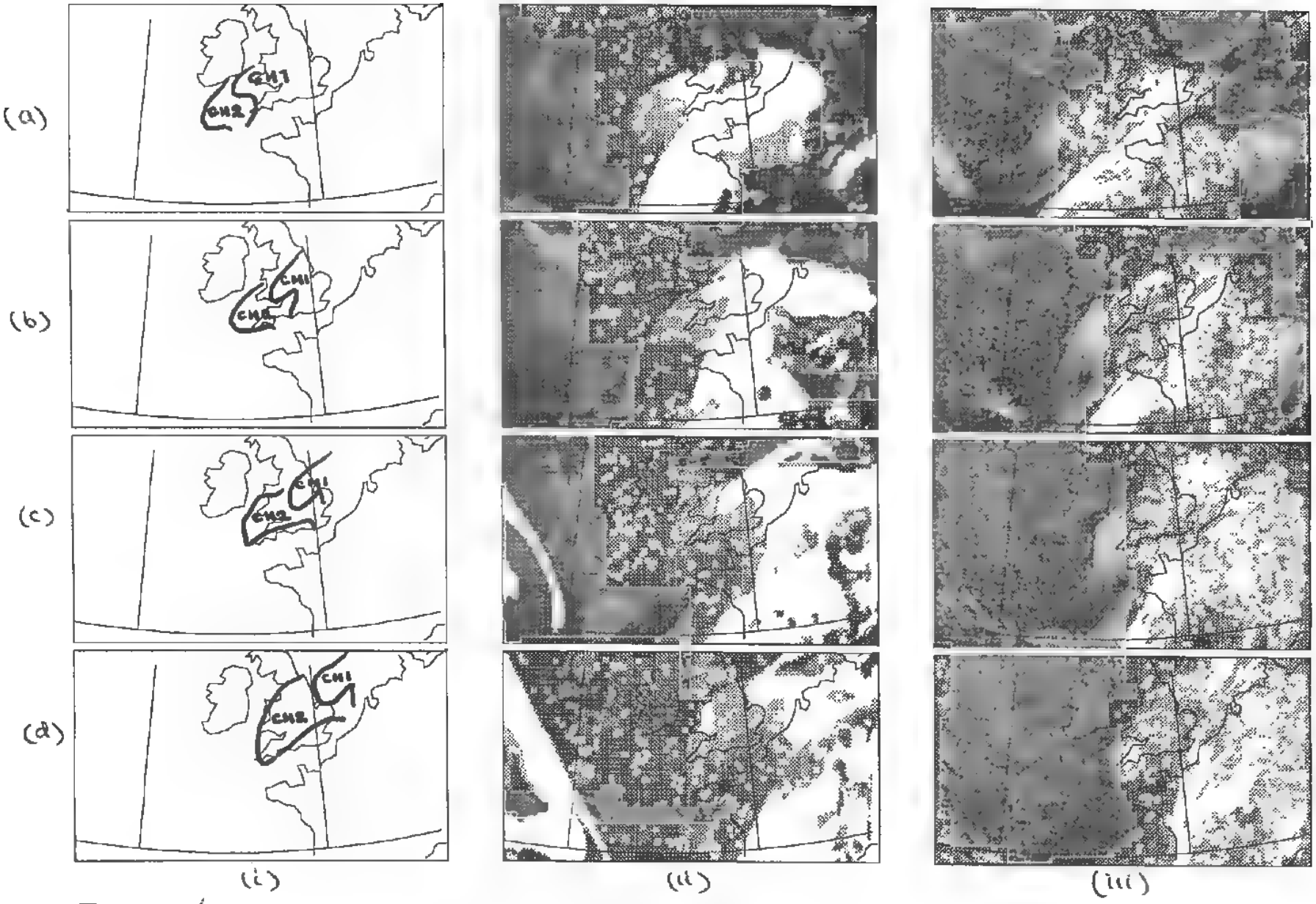

Figure 6

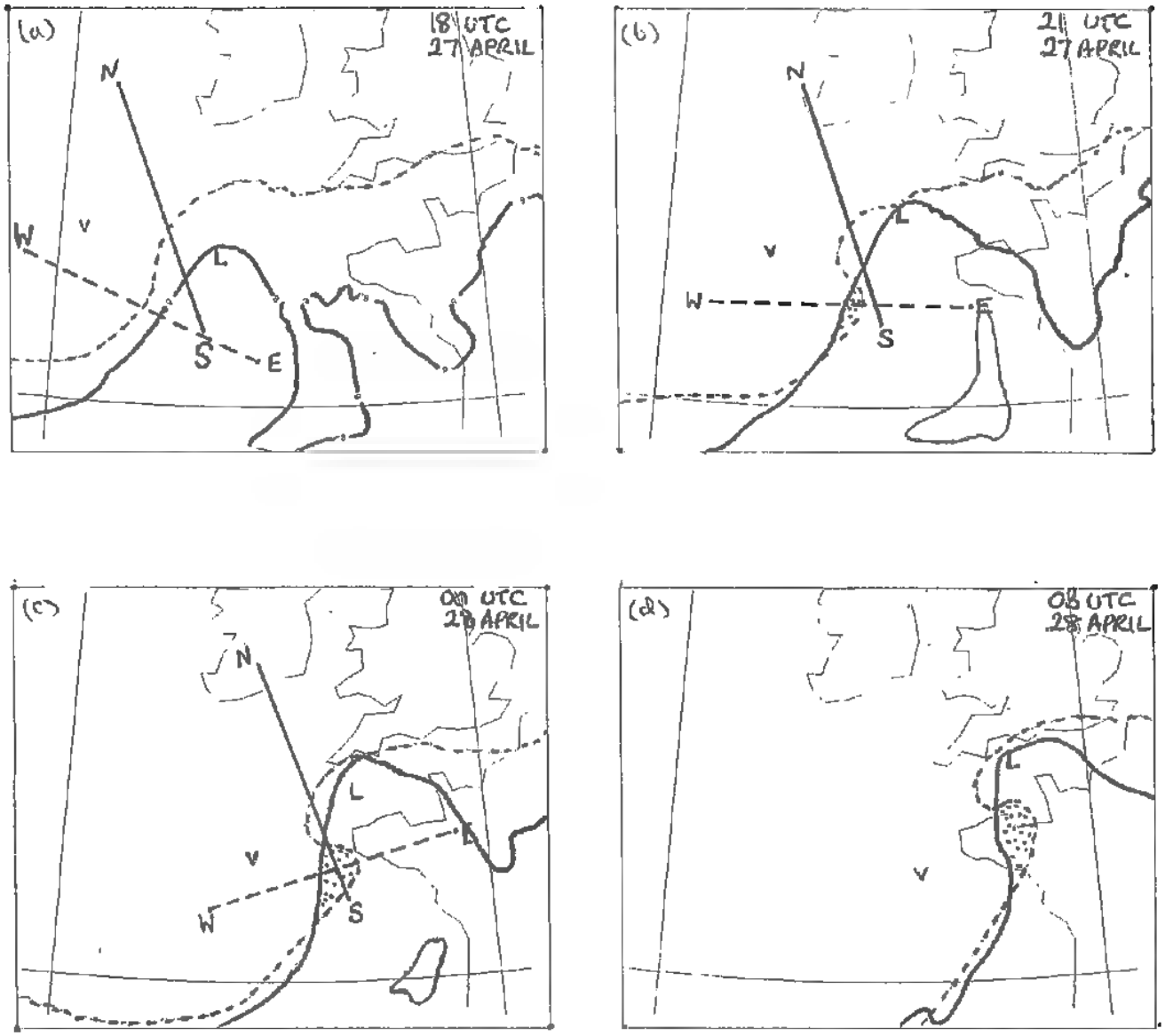
(a)
18 UTC
27 APRIL
N
W
V
L
S
E
(b)
21 UTC
27 APRIL
N
V
L
W
E
S
(c)
00 UTC
28 APRIL
N
L
V
W
S
(d)
03 UTC
28 APRIL
L
V

Figure 7

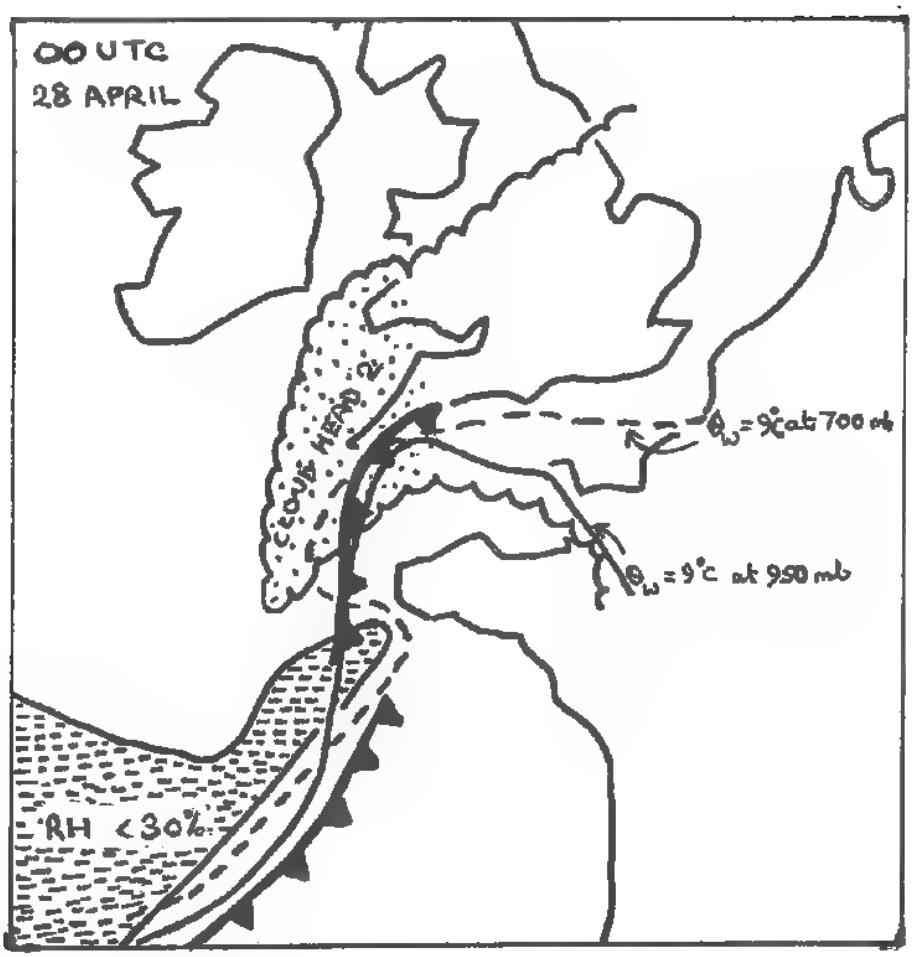
00 UTC
28 APRIL
CLOUD HEAD
θ_w = 9°C at 700 mb
θ_w = 9°C at 950 mb
RH < 30%

Figure 8

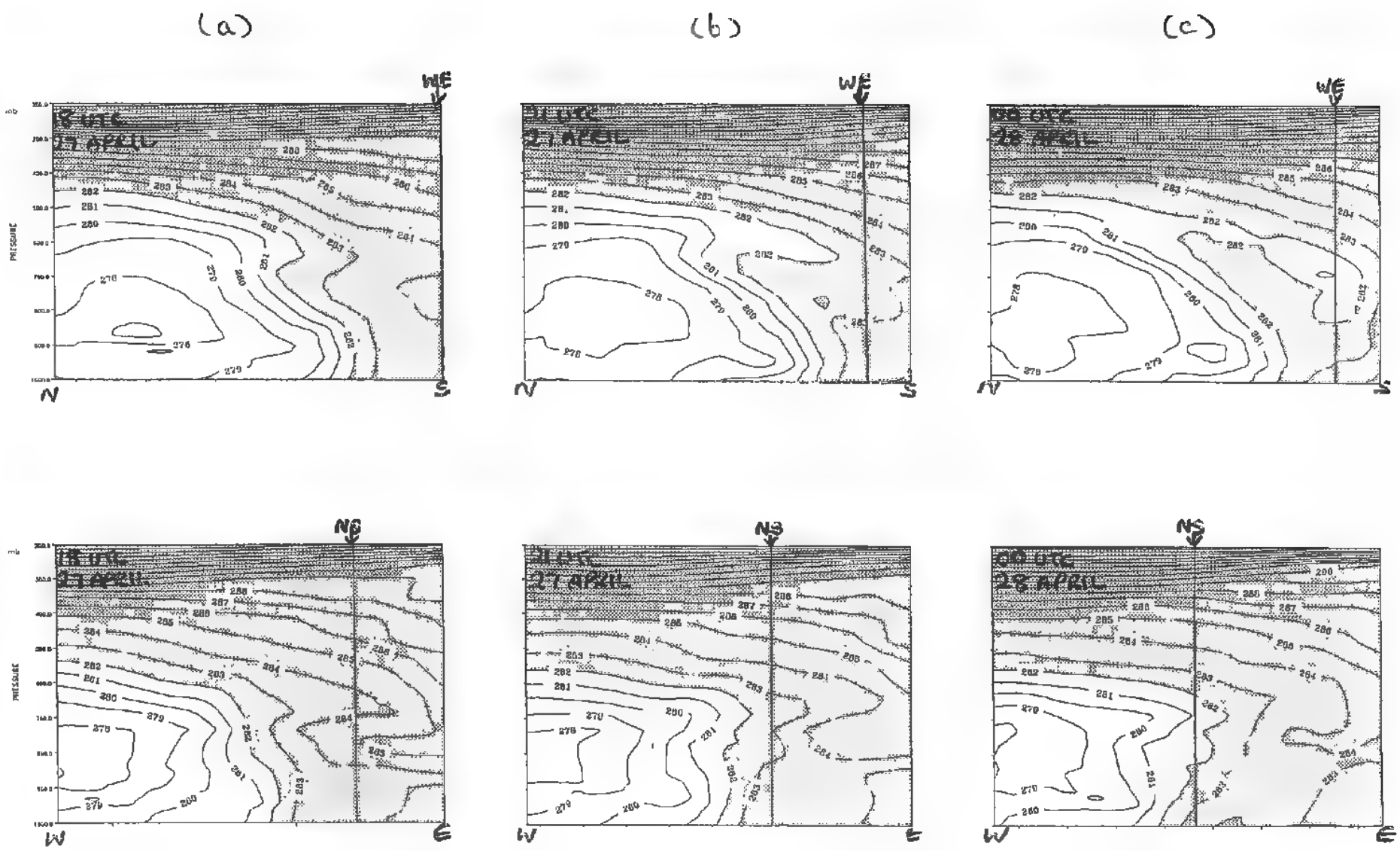

Figure 9

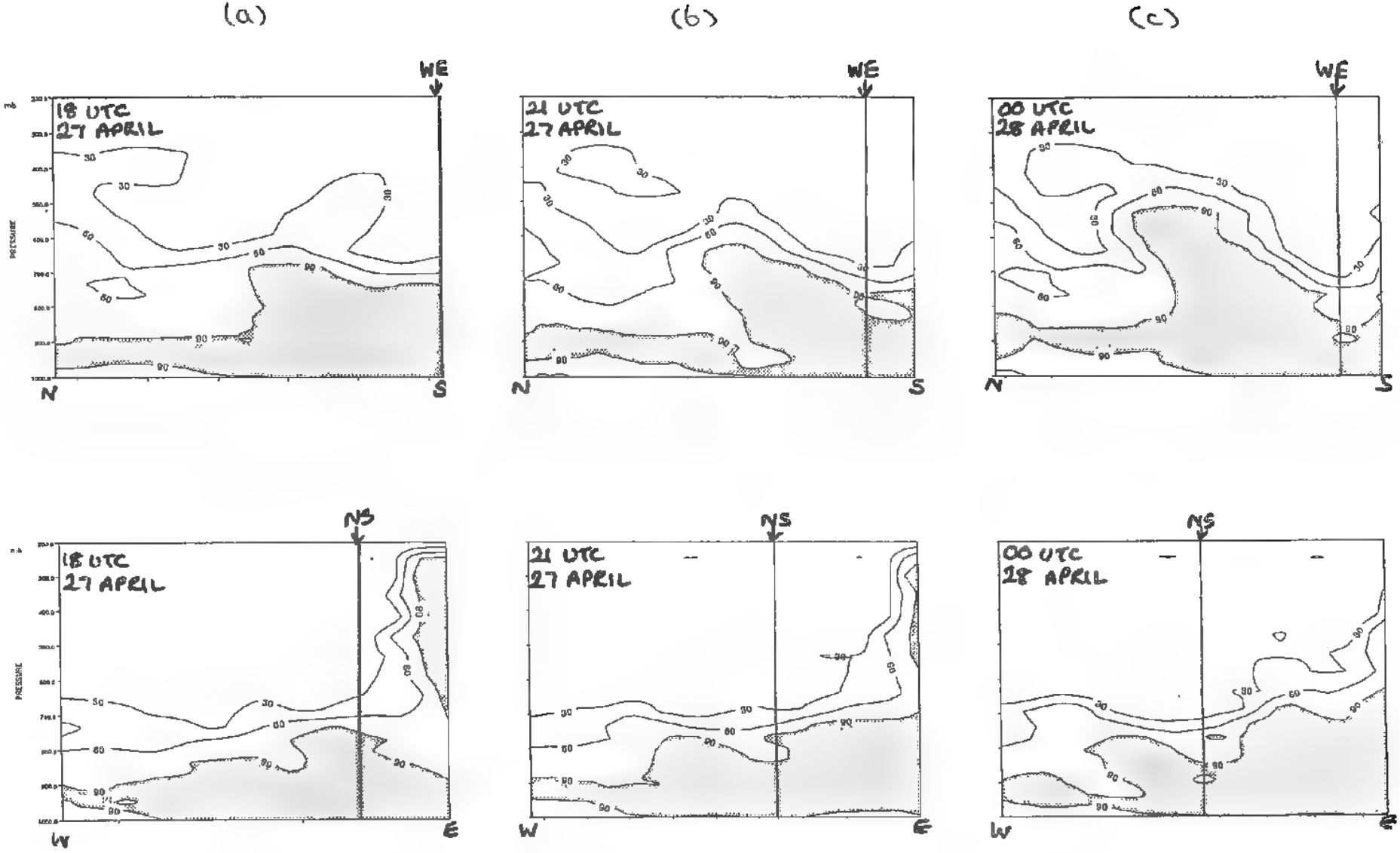
(a)
(b)
(c)
WE
18 UTC
27 APRIL
21 UTC
27 APRIL
00 UTC
28 APRIL
N
S
NS
W
E
PRESSURE

Figure 10

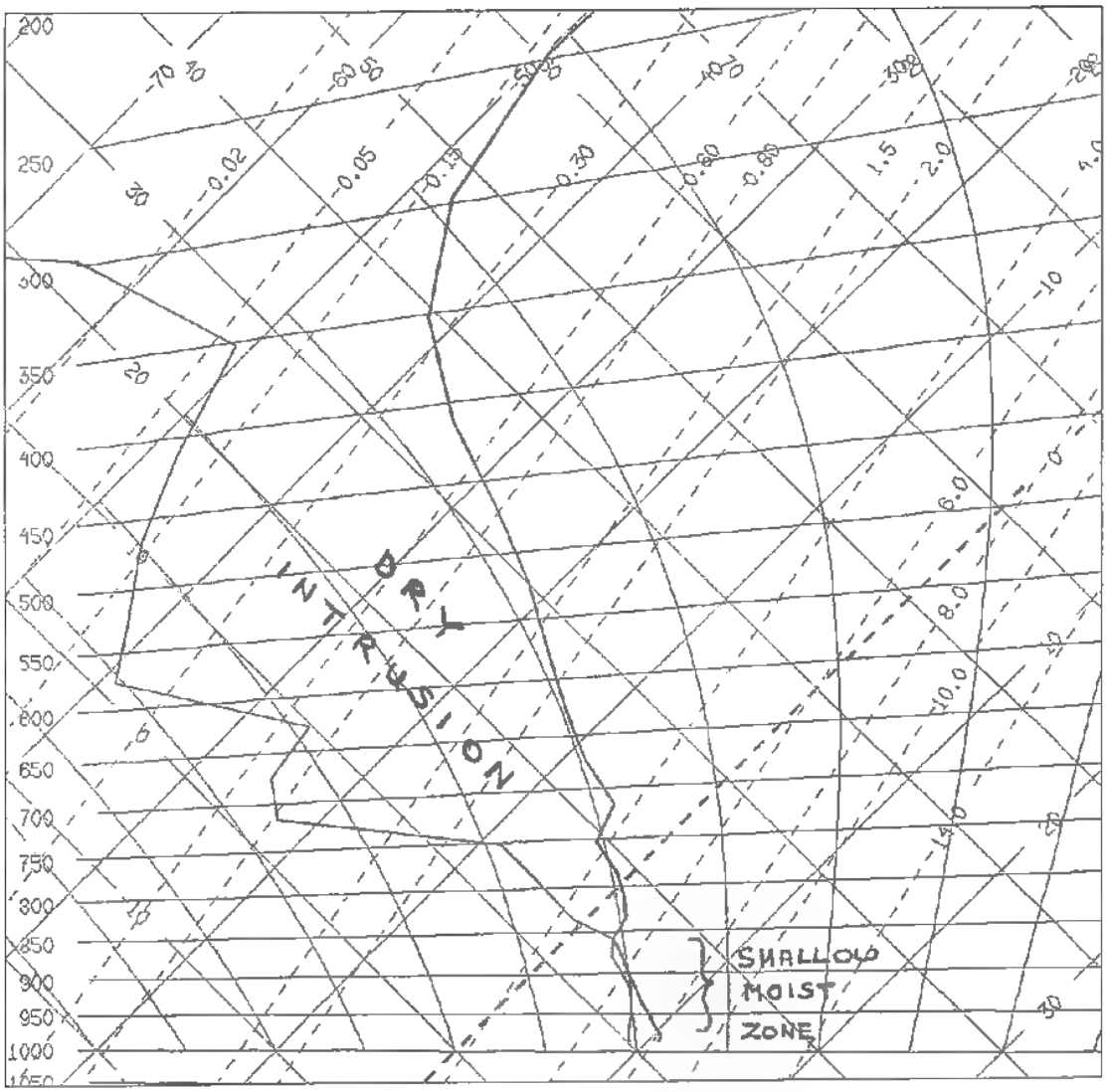

Figure 11

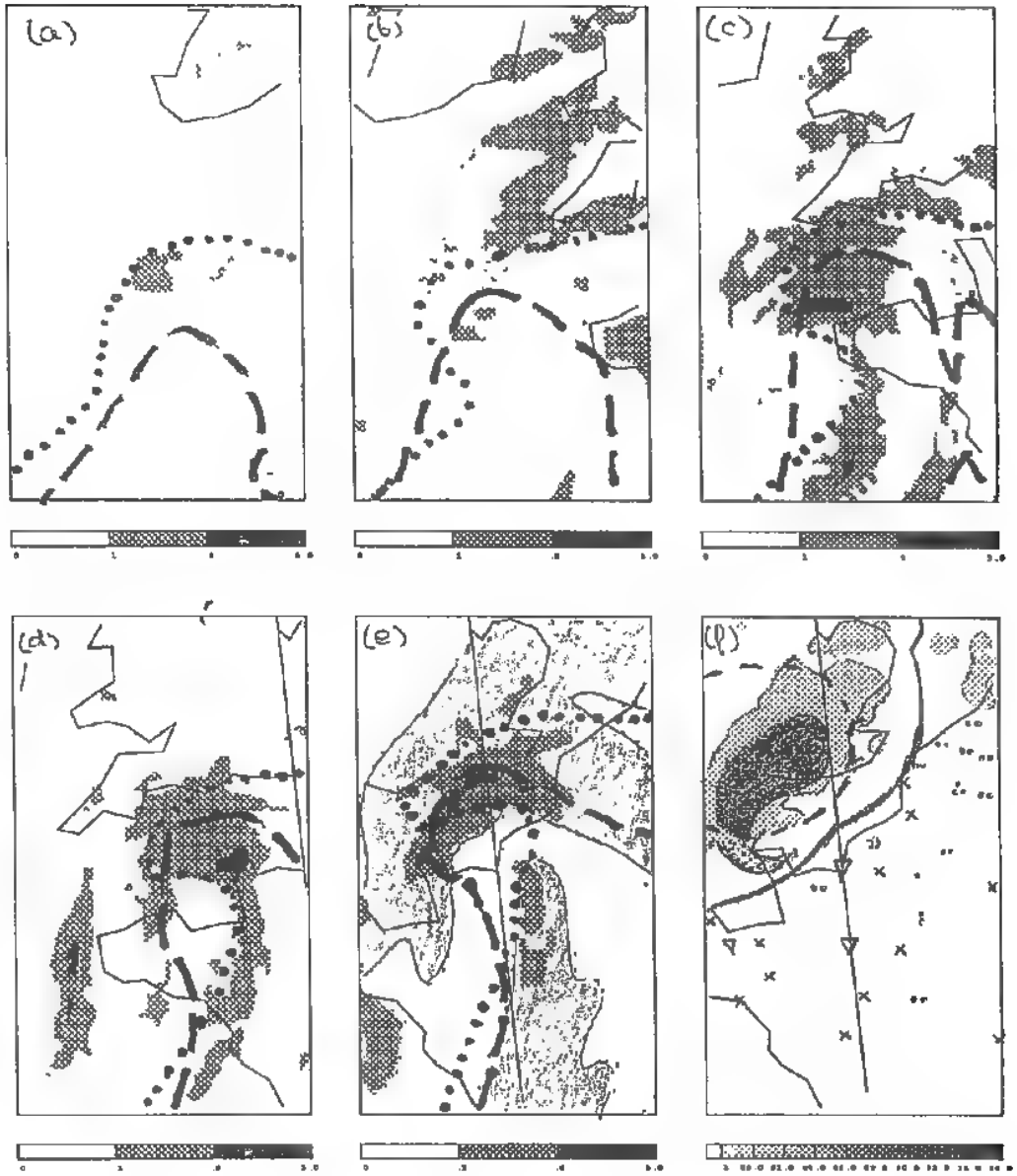

Figure 12

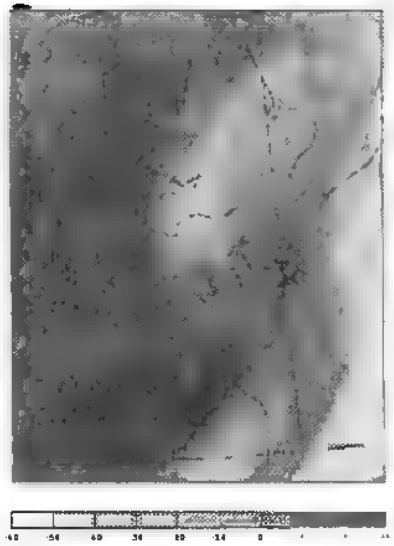

(a)

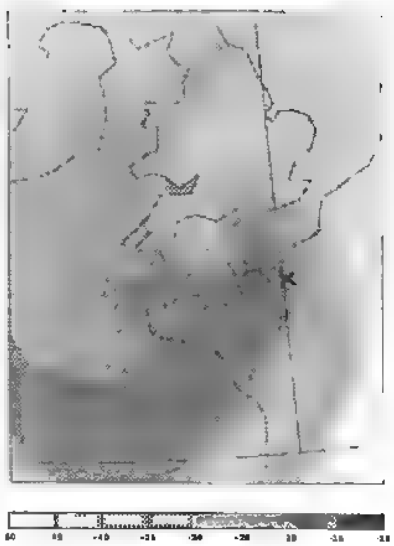

(b)

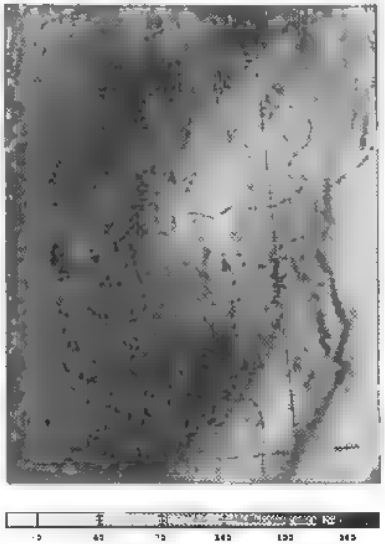

(c)

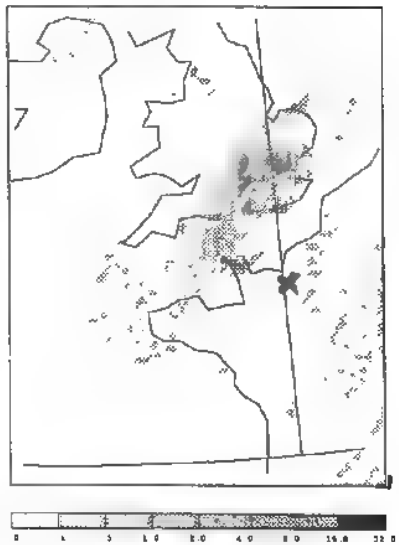

(d)

Figure 13

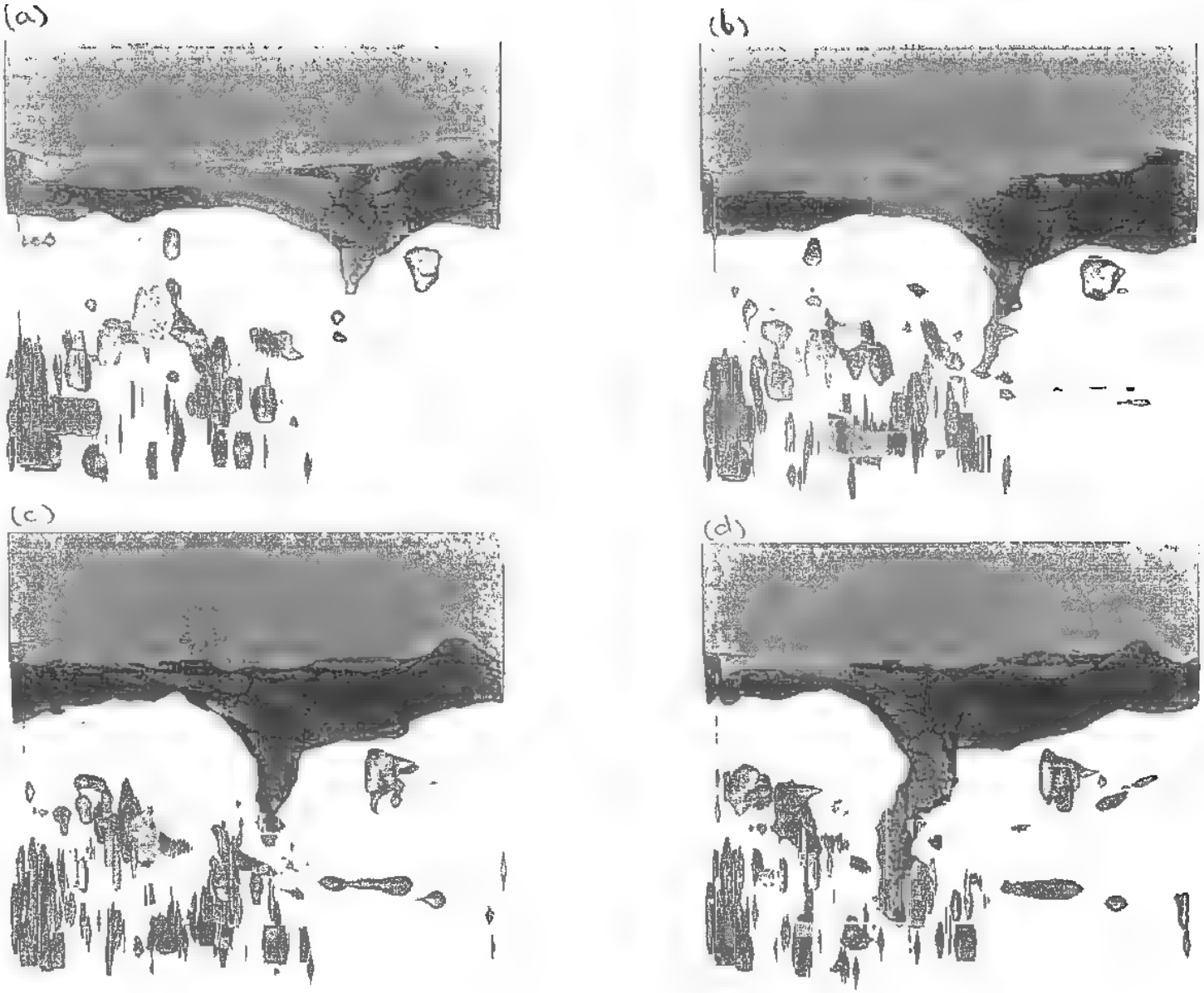

Figure 14

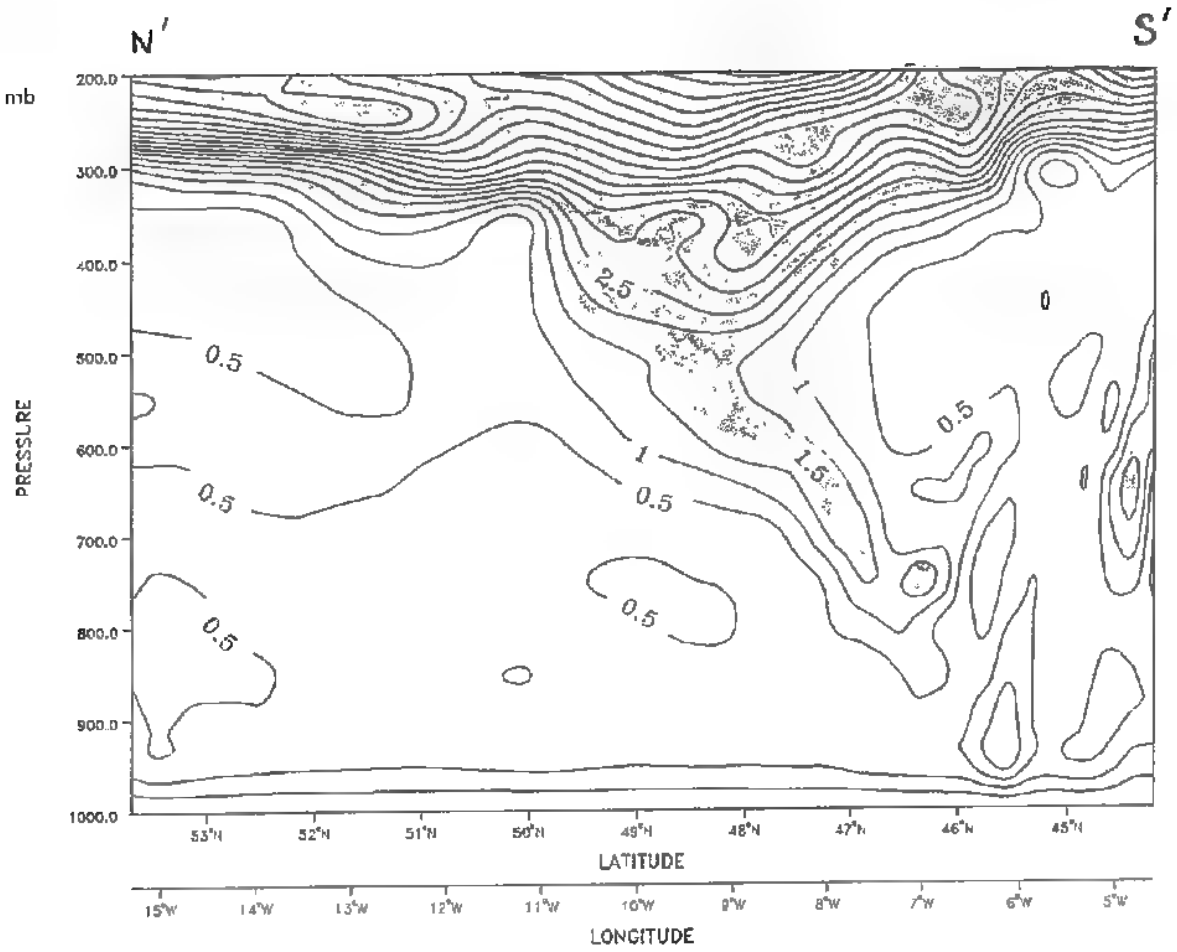
N'
S'
mb
200.0
300.0
400.0
500.0
600.0
700.0
800.0
900.0
1000.0
PRESSURE
2.5
0.5
1
1.5
0
53°N
52°N
51°N
50°N
49°N
48°N
47°N
46°N
45°N
LATITUDE
15°W
14°W
13°W
12°W
11°W
10°W
9°W
8°W
7°W
6°W
5°W
LONGITUDE

(a)

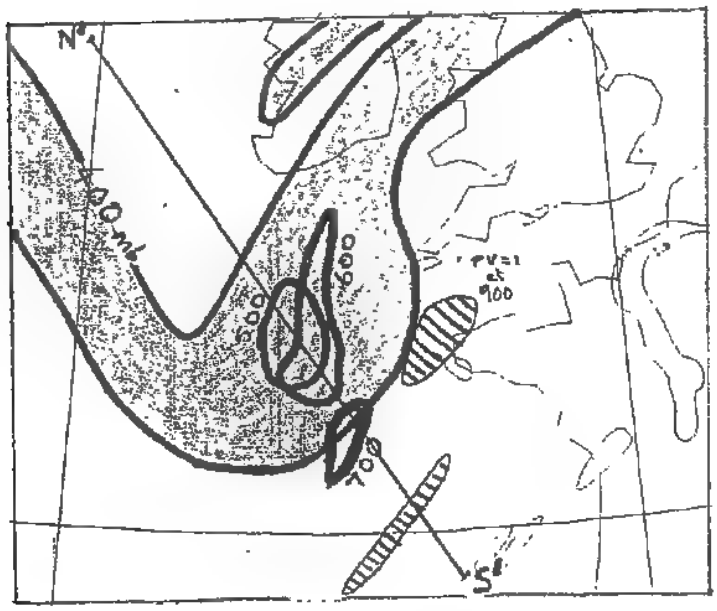
N'
400 mb
500
600
700
PV=1
at
900
S'

(b)

Figure 15

CURRENT JCMM INTERNAL REPORTS

This series of JCMM Internal Reports, initiated in 1993, contains unpublished reports and also versions of articles submitted for publication. The complete set of Internal Reports is available from the National Meteorology Library on loan, if required.

1. **Research Strategy and Programme.**
   K A Browning et al
   January 1993

2. **The GEWEX Cloud System Study (GCSS).**
   GEWEX Cloud System Science Team
   January 1993

3. **Evolution of a mesoscale upper tropospheric vorticity maximum and comma cloud from a cloud-free two-dimensional potential vorticity anomaly.**
   K A Browning
   January 1993

4. **The Global Energy and Water Cycle**
   K A Browning
   July 1993

5. **Structure of a midlatitude cyclone before occlusion.**
   K A Browning and N Roberts
   July 1993

6. **Developments in Systems and Tools for Weather Forecasting.**
   K A Browning and G Szejwach
   July 1993

7. **Diagnostic study of a narrow cold frontal rainband and severe winds associated with a stratospheric intrusion.**
   K A Browning and R Reynolds
   August 1993

8. **Survey of perceived priority issues in the parametrizations of cloud-related processes in GCMs.**
   K A Browning
   September 1993

9. **The Effect of Rain on Longwave Radiation.**
   I Dharssi
   September 1993

10. **Cloud Microphysical Processes - A Description of the Parametrization used in the Large Eddy Model.**
H Swann
July 1994

11. **An Appreciation of the Meteorological Research of Ernst Kleinschmidt.**
A J Thorpe
May 1992

12. **Potential Vorticity of Flow Along the Alps.**
A J Thorpe, H Volkert and Dietrich Heimann
August 1992

13. **The Representation of Fronts.**
A J Thorpe
January 1993

14. **A Parametrization Scheme for Symmetric Instability: Tests for an Idealised Flow.**
C S Chan and A J Thorpe
February 1993

15. **The Fronts 92 Experiment: a Quicklook Atlas.**
Edited by T D Hewson
November 1993

16. **Frontal wave stability during moist deformation frontogenesis. Part 1. Linear wave dynamics**
C H Bishop and A J Thorpe
May 1993

17. **Frontal wave stability during moist deformation frontogenesis. Part 2. The suppression of non-linear wave development.**
C H Bishop and A J Thorpe
May 1993

18. **Gravity waves in sheared ducts.**
S Monserrat and A J Thorpe
October 1993

19. **Potential Vorticity and the Electrostatics Analogy: Quasi-Geostrophic Theory.**
C Bishop and A J Thorpe
November 1993

20. **Recent Advances in the Measurement of Precipitation by Radar.**
A J Illingworth
April 1993

21. **Micro-Physique et Givrage. Cloud Microphysics and Aircraft Icing.**
A J Illingworth
May 1993

22. **Differential Phase Measurements of Precipitation.**
M Blackman and A J Illingworth
May 1993

23. **Estimation of Effective Radius of Cloud Particles from the Radar Reflectivity.**
N I Fox and A J Illingworth
May 1993

24. **A Simple Method of Dopplerising a Pulsed Magnetron Radar.**
L Hua, A J Illingworth and J Eastment
November 1993

25. **Radiation and Polar Lows.**
George C Craig
February 1994

26. **Collected preprints submitted to International Symposium on the Life Cycles of Extratropical Cyclones; Bergen, Norway, 27 June - 1 July 1994**
April 1994

27. **Convective Frontogenesis**
Douglas J Parker and Alan J Thorpe
April 1994

28. **Improved Measurement Of The Ice Water Content In Cirrus Using A Total Water Evaporator**
Philip R A Brown and Peter N Francis
April 1994

29. **Mesoscale Effects of a Dry Intrusion within a Vigorous Cyclone**
K A Browning and B W Golding
April 1994

30. **GEWEX Cloud System Study, Science Plan**
May 1994

31. **Parametrization of Momentum Transport by Convectively Generated Gravity Waves**
R Kershaw
February 1995

32. **Mesoscale Modelling Newsletter, No. 5**
May 1994

33. **Observations of the mesoscale sub-structure in the cold air of a developing frontal cyclone**
K A Browning, S A Clough, C S A Davitt, N M Roberts and T D Hewson
May 1994

34. **Longwave Radiative Forcing of a Simulated Tropical Squall Line**
Imtiaz Dharssi
July 1994

35. **On the nature of the convective circulations at a kata-cold front**
K A Browning
September 1994

36. **Collected preprints of papers submitted to the COST-75 International Seminar on Advanced Weather Radar Systems, Brussels, 20-23 September 1994**
November 1994

37. **Use of satellite imagery to diagnose events leading to frontal thunderstorms: Parts I and II of a case study**
K A Browning and N M Roberts
November 1994

38. **The role of spaceborne millimetre-wave radar in the global monitoring of ice cloud**
P R A Brown, A J Illingworth, A J Heymsfield, G M McFarquhar, K A Browning and M Gosset
December 1994

39. **Potential Vorticity Inversion**
Michal Ziemianski
October 1994

40. **Theory of mature tropical cyclones; A comparison between Kleinschmidt (1951) and Emanual (1986)**
Suzanne L Gray
December 1994

41. **Dispersion and removal of pollutants during the passage of an atmospheric frontal system**
N R Gimson
December 1994

42. **The role of snow sublimation in frontogenesis**
D J Parker and A J Thorpe
December 1994

43. **Potential vorticity and the electrostatics Analogy: Ertel-Rossby formulation**
A J Thorpe and C H Bishop
December 1994

44. **Mesoscale aspects of extratropical cyclones: an observational perspective**
K A Browning
January 1995

45. **A Polar Low Outbreak: Evolution and Mesoscale Structures**
T D Hewson, G C Craig and C Claud
February 1995

46. **Generation of near-surface gusts by deep convection**
K Nakamura and R Kershaw
April 1995

47. **Attribution concepts applied to the omega equation**
S A Clough, C S A Davitt and A J Thorpe
June 1995

48 **Parametrization of mixed-phase cloud and precipitation**
Susan P Ballard and M Gerard Hutchinson
June 1995

49 **Short-range forecasting of stratocumulus: Initialization V Prediction**
Susan P Ballard, Simon D Jackson and B Macpherson
June 1995

50 **Contributions of the JCMM/Dept of Meteorology Radar Group to the 27th AMS Radar Meteorology Conference, Vail October 1995**
June 1995

51 **Cold pools in shear**
Douglas J Parker
September 1995

52 **High-resolution analysis of frontal fracture**
K A Browning, S P Ballard and C S A Davitt
September 1995

Met Office Joint Centre for Mesoscale Meteorology Department of Meteorology
University of Reading PO Box 243 Reading RG6 6BB United Kingdom
Tel: +44 (0)118 931 8425 Fax: +44 (0)118 931 8791
www.metoffice.com